Supporting Online Material for

Developmental Patterning by Mechanical Signals in *Arabidopsis*

Olivier Hamant, Marcus Heisler, Henrik Jönsson, Pawel Krupinski, Magalie Uyttewaal, Plamen Bokov, Francis Corson, Patrik Sahlin, Arezki Boudaoud, Elliot M. Meyerowitz,* Yves Couder,* Jan Traas*

*To whom correspondence should be addressed. E-mail: jan.traas@ens-lyon.fr (J.T.); meyerow@caltech.edu (E.M.M.); couder@lps.ens.fr (Y.C.)

Published 12 December 2008, *Science* **322**, 1650 (2008)
DOI: 10.1126/science.1165594

This PDF file includes:

Other Supporting Online Material for this manuscript includes the following:

Supporting Online Material

Material and Methods

Plant Material and Growth Conditions

The *p35::GFP-MBD, p35S::LTI6b-GFP, pFIL::DsRED-N7* and *pBOUND-GFP Arabidopsis* lines have been described previously (*S1-S3*). For NPA treatment, 10 µM napthylphthalamic acid was added to the medium. As soon as naked inflorescences had formed, the plants were transferred to medium without inhibitor.

Oryzalin treatments

Whole plantlets were transferred in boxes containing solid medium without NPA, and attached by adding a lukewarm gel agarose at 0.5%. The plantlets were immersed in an aqueous solution containing oryzalin at 10 to 20 µg/mL for three hours, and then washed in water twice for 15 min on day 1. The same treatment was applied on day 2, and images of the meristem were obtained from day 1 to day 5.

Laser ablation

Laser ablation of meristem cells was accomplished using a Photonics Instruments MicroPoint laser system consisting of a pulsed Nitrogen laser coupled to a dye cell containing Coumarin 440. This resulted in an output wavelength of 440 nm that was pulsed at 6 Hz and gated using a foot pedal. We used a variable neutral density filter to attenuate the output until single cells could be targeted without damage to neighboring cells, as assessed by subsequent FM 4-64 staining (50 µg/ml). Cells were targeted visually by positioning them, using the stage controls, such that they were aligned under the eyepiece cross hairs. Two to three bursts of up to a

second were used to kill each cell. The observation of the collapse of the cell was used to confirm that ablation had occurred.

Confocal Microscopy and Image analysis

Meristems were examined with an inverted or an upright LSM-510 Laser-Scanning Confocal Microscope (Zeiss, Jena, Germany) as described previously *(S4, S5)*. Projections of the signal in the L1 layer were obtained using the Merryproj software *(S6)*. The cortical microtubules orientations and growth measurements were analyzed with the ImageJ software (http://rsb.info.nih.gov/ij/). All calculations were performed using Microsoft Excel 2007.

Figure S1. **Schematic representation of the main conclusion**

Figure S2. ***pBOUND-GFP* after microtubule depolymerization**

The kinetics of *pBOUND-GFP* induction after oryzalin treatment shows that the depolymerization of the microtubule does not affect the pattern of expression of this boundary marker and does not alter the phyllotactic pattern, while preventing the formation of a crease between the meristem and the young primordia. The image of the surface is obtained by reflection using a confocal microscope. Scale bar: 50 µm

Figure S3. **Impact of microtubule depolymerisation on meristem shape**

A. 3 days after microtubule depolymerization, the tip of the stem of a *GFP-LTI6b* line switched from a pin-shaped to a balloon-shaped structure. A white arrowhead indicates the same cell at t0 and t72h. Scale bar: 20 µm

B. Simulation of an oryzalin-treated growing stem. Microtubular contribution to the mechanics is removed and results in an expanded tissue, mainly at the apex.

C. Simulation of an oryzalin-treated experimental template. The template from Figure 3C is first simulated with microtubular contribution and stress feedback, and then the microtubular contribution to the mechanics is removed. Cells expand elastically, and the crease is lowered to some degree in this simulation with no wall growth. For a comparison, the long term impact of oryzalin on crease shape is shown on figure 1B and 1D.

Figure S4. **The cortical microtubules alignment follows the phyllotactic pattern**

Top panels show a living meristem followed during 72h. Lower panels describe microtubule orientations in the same meristem. Cell geometry was represented as described in (*S6*) and the orientation of the microtubules in each cells of living *GFP-MBD* meristems was manually determined. A color code was then applied to these orientations: red, for cells with microtubules parallel to the x axis, green, for cells with microtubules at 60° with the x axis, and blue for microtubules at 120° with the x axis. The distribution of colors in the case circumferential microtubules is given in the legend, the microtubules orientation being drawn as white lines. In a naked, pin shaped meristem (t=0h), each color is roughly equally represented indicating the orthoradial orientation of the microtubules. When primordia are initiated, one color dominates the others (t=48h: blue-green, t=72h: red). Scale bar: 20 µm

Figure S5. **Description of the mechanical models**

A,B The simplified three-dimensional model. The potential (equation S1 in Note S1) leads to forces F_w, F_t, and F_{int} as depicted in A. Mechanical anisotropy is introduced from a microtubular direction defined for the cells. Walls more parallel to the microtubules direction are stiffer as illustrated by thicker walls in B (see Note S1).

C. Cross-section of the cell-layers used in the Finite Element Model (see Note S2).

Figure S6. **Mechanical simulations of differently shaped templates**

The two-dimensional stress feedback model simulated on two half-sphere shaped (**A**) and one saddle-shaped (**B**) synthetic templates. Bars show the microtubule directions within the cells. The general patterns agree with our theoretical discussion in the main text. Note the cell dependence on the half-sphere templates. In the very symmetric case (left) the circumferential alignment reach closer to the apex compared to the template with less symmetric cell positions and shapes (right). The weak anisotropy close to the apex results in a weaker geometrical dependence and in general more random and instable directions. The anisotropy is quantified and colored in a FEM simulation on a half-sphere template (**C**).

Figure S7. **Laser-induced cell ablation experiment in the boundary**

A. Pattern of tensile stresses obtained from FEM simulation of ablation in the boundary region with highly ordered initial stress pattern. Direction of tensile stresses in the top walls of tissue before (left) and after (right) ablation. Maximal principal tensile stress direction aligns along positive curvature of the tissue.

B. Close-up from **A**

C. *GFP-MBD* expression in the L1 layer in the boundary 7h30 after ablation. Arrows point to cells which maintain tangential microtubules orientation at the boundary after ablation. Scale bar: 5 µm

Figure S8. **Two-cell ablation experiment**

A. Principal stress pattern at the outer surface of the meristem obtained from the FEM simulation of a two-cell ablation experiment before ablation.

B. Principal stress pattern at the outer surface of the meristem obtained from the FEM simulation of a two-cell ablation experiment after ablation. Cell walls as well as turgor pressure from affected cells are removed in the simulation. The stress pattern is circumferential to each of the ablated regions and in particular stress alignment is enhanced in the cell between two removed cells.

C. *GFP-MBD* expression in the L1 layer in the central zone after a two-cell ablation. Scale bar: 5 µm

Figure S9. S**tabilization of cortical microtubule orientation following compression**

A. *GFP-MBD* expression in the L1 layer of a meristem before the application of the constraint, at t0 and 3h30min after the application of the constraint. After the release of the constraint, the meristem recovers its original shape (t6h:Release) and initiates organs normally (t6h + Release 68h). Scale bar: 20 µm

B. *GFP-MBD* expression in the L1 layer of a meristem at t0 and 3h30min after the application of the constraint. Most cells switch from random microtubules orientation at t0 to a single microtubule orientation 3h30min later. Scale bar: 5 µm

Figure S10. **Cortical microtubule reorientation following compression**

The spring progressively compressed the meristem from t0 to t6h. The enrichment in the number of cells displaying microtubules with an angle between 0-45° is visible as in Figure 4, after t6h. Note the decrease in the number of cells with unstable microtubules over time (green histograms). Scale bar: 20 µm

The calculated stress in the compressed meristems is as follows: our mechanical model consists of a half-sphere bound to a cylinder of radius R. Two opposite forces of magnitude F, directed along x, are applied at two opposite points at the equator, resulting in a displacement d of these points. The stresses at the apex can be computed from the superimposition of the isotropic stress $\sigma_{xx}^{0} = \sigma_{yy}^{0} = PR/2$ due to the turgor, and of stress field induced by the two forces. This additional stress is anisotropic, $\sigma_{yy}^{A} = -\sigma_{xx}^{A} = F/(2\pi R)$ (*S7*). Relating force to the displacement d involves the thickness h of the outer layer, its elastic modulus E, and its Poisson ratio ν. We compute $F(d)$ in the limit that the contact zone is smaller than R: $F=\pi Ehd^2/(1-\nu)/R/2$. This yields the total stress: the stress perpendicular to the force, $\sigma_{yy}=PR/2+Eh(d/R)^2/(1-\nu)/4$, is higher than the stress in the direction of the force, $\sigma_{xx}=PR/2-Eh(d/R)^2/(1-\nu)/4$. The anisotropy of stress becomes $\delta=(E/P)\,(h/R)\,(d/R)^2/(1-\nu)$.

Using images from compressed meristems, we estimate $h/R \approx 0.1$, $d/R \approx 0.4$. For onion epidermal cells, Wei *et al.* (*S8*) measured $\nu \approx 0.2$ and E in the range $10P$ to $30P$. For meristems, which are soft tissues, we take the lower value $E \approx 10P$. As a result $\delta \approx 0.2$ – the stress is weakly anisotropic. This weak anisotropy might be sensitive to the details of the walls positions and orientations.

Figure S11: **Microtubule behavior in individual cells after compression**

The microtubule orientations were measured in a total of 489 individual cells from 13 compressed meristems (3 to 8 time points per meristem). t0 corresponds to 0 hour after compression. If the cell exhibited one major microtubule orientation at t0 (307 cells), the reorientation of the microtubules was measured in individual cells by subtracting the microtubule angle after 4 to 12 hours of compression to the microtubules angle at t0 (A). If the cell exhibited multiple orientations at t0 (182 cells), the microtubule orientation was measured after 4 to 12 hours of compression (B).

A. Microtubule reorientations after compression in cells which exhibited one major microtubule orientation at t0: Blue: percentage of cells with microtubule reorientations superior to 10° towards the axis perpendicular to the blades, Red : percentage of cells with microtubule reorientations more than 10° towards the axis parallel to the blades; Green: percentage of cells with microtubule reorientations less than 10°.

B. Microtubule orientations after compression in cells which exhibited multiple microtubule orientations at t0: Blue: percentage of cells acquiring a microtubule orientation rather perpendicular to the blades (angle between 55 and 90°), Red : percentage of cells acquiring a microtubule orientation rather parallel to the blades (angle between 0 and 35°), Green: percentage of cells acquiring microtubule orientation of 45+/-10° with the blades or maintaining multiple microtubule orientations after compression.

Movie S1: **Two types of cortical microtubule behaviors in the shoot apex**

Aligned confocal projections showing *p35S::GFP-MBD* expression every 10 minutes over a 2 hr and 20 min period. In the center, cells exhibit either stable or unstable microtubules orientation over a short period of time, whereas at the boundary the microtubules orientation is maintained parallel to the boundary.

Movie S2: **Simulation of a growing primordium on the flank of a meristem**

Movie S3: **Simulation a growing pin-shaped meristem**

Movie S4: **Cortical microtubules reorient following laser-induced cell ablation**

Movie S5: **Cortical microtubules reorient following tangential stretch in the meristem**

Aligned confocal projections showing *p35S::GFP-MBD* expression before and 6 hours after the application of a lateral compression. The sequence is repeated five times to better see the cell shape changes and microtubules reorientations.

Movie S6: **Cortical microtubules reorient following tangential stretch in the meristem**

Aligned confocal projections showing *p35S::GFP-MBD* expression at t0 and 6 hours after the application of a lateral compression, showing that the measurement of the microtubule reorientation is not biased by the geometrical deformation of the meristem.

Note S1: **Two-dimensional mechanical model**

A simplistic two-dimensional tissue model representing the L1 layer of cells was designed. The model is based on the assumption that cell walls hold the forces generated from an internal pressure from the cell tissue, where a potential energy is defined by

$$U = \sum_{w \in walls} \frac{k_w}{2}\left(\frac{l_w - l_w^0}{l_w^0}\right)^2 - \sum_{c \in cells} P_c A_c - \sum_{c \in cells} P_{c,\mathrm{int}} V_{c,\mathrm{int}} . \qquad \text{(S1)}$$

Walls are assumed to be elastic three-dimensional elements with constant thickness (t) and depth (d), and linear elastic properties E_w, which results in a one-dimensional spring model where $k_w = t\ d\ E_w$. The actual and relaxed wall lengths are given by l_w and l_w^0 repectively, and the resulting forces, F_w, act along the one-dimensional spring direction (Fig. S5).

Internal pressure gives rise to two forces, where the forces between cells of the L1 layer ($F_{t,cw} = P_c\ d\ l_w$) acting perpendicular to the wall is canceled with the assumption of equal pressure in all cells. The force from the internal tissue is given by $F_{c,\mathrm{int}} = P_{c,\mathrm{int}}\ A_c$, where A_c is the cell

area and acts perpendicular to the two-dimensional cell plate (Fig. S5A). Note that this is a simplification of the combined forces acting on the epidermal cell layer from the internal tissue, but it has the property to act perpendicular to the contact surface between the internal and epidermal tissue.

Mechanical anisotropy is introduced in the model by defining a microtubule direction for each cell $\boldsymbol{n}_c$. The spring constant for a cell wall k_w is a function of the microtubules and wall direction, $\boldsymbol{n}_w$ described by

$$k_w = k_{\min} + k_{\max} (\boldsymbol{n}_w \cdot \boldsymbol{n}_c)^2 = k_{\min} + k_{\max} \cos^2(\Theta)$$

where $k_{\min}$ is the isotropic contribution and $k_{\max}$ is the anisotropic contribution. The squared scalar product results in the factor $\cos^2(\Theta)$ where Θ is the angle between the cortical microtubule direction and the wall direction ($\Theta \leq 90$ deg.) in the cell. Since each wall has two cell neighbors, the $k_{\max}$ contribution is the sum for the two cells, $0.5\ k_{\max}$ ($\cos^2(\Theta_1) + \cos^2(\Theta_2)$), where the two angles (Θ_1, Θ_2) are between the microtubules directions of the two cells and the wall direction.

Stress feedback is implemented by updating the microtubule direction for a cell by the directional weighted average of the wall stresses. We use circular statistics with a periodicity of 180 deg, and the average is calculated by

$$\Theta_c = \frac{1}{2} a\tan\left(\frac{\sum_w F_w \sin(2\Theta_w)}{\sum_w F_w \cos(2\Theta_w)} \right) \qquad \text{(S2)}$$

where Θ_c (Θ_w) is the directional angle for the cell (wall). The directions are updated with a delay, such that $n_c^{new} = (1-\alpha\Delta t)n_c^{old} + \alpha\Delta t n_c$, where $\boldsymbol{n}_c^{\text{new}}$ is the new direction, $\boldsymbol{n}_c^{\text{old}}$ is the previous direction, $\boldsymbol{n}_c$ is the feedback direction from Eq. S2, α is a delay parameter and Δt is the time step.

Plastic tissue growth is obtained by adding material to walls under tension, i.e. increasing the resting length of walls stretched above a threshold following the dynamics

$$\frac{dl_w^0}{dt} = k_g\left(\frac{l_w - l_w^0}{l_w^0} - T_g\right)$$

if $\left(\frac{l_w - l_w^0}{l_w^0} - T_g\right) > 0$ and $\frac{dl_w^0}{dt} = 0$ otherwise.

Since k_g is constant, individual wall growth rates result from different $\Delta l_w = (l_w - l_w^0)/l_w^0$. Different values of Δl_w originate from the applied forces (pressure and wall-wall interactions), and the dynamics of k_w. Hence there is no explicit relation between maximal stress and maximal growth direction in the model, and it can produce maximal growth along the maximal stress direction as well as perpendicular to it depending on the stress patterns.

Cell division occurs when cells reach a threshold size, $A_c^{\max}$, and is implemented by adding a new wall through the center of mass of the cell, and in a direction parallel to the microtubules direction of the cell. To avoid too short cell walls and 4-vertices, the connection of the new wall to old walls are moved to a minimal distance $0.3l_w$ from an existing vertex (along wall w).

In the tip growing simulation a spatial factor is added to the growth rate, k_g, replacing the constant with a function of the distance, d, from the wall to the most apical vertex position

$$k_g \rightarrow k_g \frac{K_g^{n_g}}{K_g^{n_g} + d^{n_g}}$$

In the primordia growth simulations, 'auxin concentration' is used to decrease wall stiffness, which leads to bulging primordia. An auxin-dependent factor is added to the wall stiffness according to

$$k_w \rightarrow k_w \left(\frac{K_a^{n_a}}{K_a^{n_a} + a_{c1}^{n_a}} + \frac{K_a^{n_a}}{K_a^{n_a} + a_{c2}^{n_a}} \right)$$

where a_{c1} and a_{c2} are the auxin concentrations in the neighboring cells.

In all simulations, model parameter values used are: k_{min}=0.01, k_{max}=0.1, $P_{c,int}$=0.0005, and α=0.1. For the tip and primordia growth simulations the growth and division parameters are k_g=0.001, T_g=0.01, and A_c^{max}=1.5. The spatial parameters for the tip growth simulations are K_g=4 and n_g=2. The auxin dependent parameters for the primordia simulations are K_a=0.5 and n_a=2, where the 'auxin concentrations' in the primordia cells were set to 1 and 2.

Note S2: **Finite element model**

The FEM model consists of two layers of polyhedral cells connected rigidly at the walls in accordance with symplastic nature of deformation of plant tissues (Fig. S5C). In our model we considered only plant walls as the structurally strong element which bears stresses and

strains from the deformation. We assumed an isotropic elastic material for the walls. This assumption is justified for the cells on the top of shoot apical meristem which do not show aligned microtubule and microfibril orientation and thus do not exhibit anisotropic properties. The cells on the boundary of the meristem and in particular cells in the depression between the meristem and the outgrowing primordia manifest strongly aligned microtubules and are expected to behave mechanically like an anisotropic material. In this regard the use of an isotropic material in our FEM model is a simplification, which allows us to emphasize the dependence of the stress response on the geometrical shape of the tissue. The outer wall of the meristem is stronger than inner walls, which is depicted in the model by increased, two to five times comparing to inner walls, elastic modulus of the outer wall. Each cell was subject to the same turgor pressure which we picked in the range 0.1-0.4 MPa. Young's modulus of the wall material was set in the range 100-400 MPa. Tension in the L1 layer resulting from expansion of inner tissue was simulated either by stretching the whole layer or applying a uniformly distributed load on the bottom surface of the layer. Given the curvature of the model L1 layer both procedures gave the same results in terms of predicted stress pattern in the outer layer. The FEM analysis was performed with 8-node solid hexahedral elements. Ablation experiments were simulated by loss of the turgor in damaged cells and decay of the walls of ablated cells was represented by successive lowering of the Young's modulus of the walls material to the point where ablated cells are effectively removed from the model.

Supplementary References

S1. M. G. Heisler *et al.*, *Curr Biol* **15**, 1899 (Nov 8, 2005).
S2. J. Marc *et al.*, *Plant Cell* **10**, 1927 (Nov, 1998).
S3. Y. Deveaux *et al.*, *Plant J* **36**, 918 (Dec, 2003).
S4. O. Grandjean *et al.*, *Plant Cell* **16**, 74 (Jan, 2004).
S5. G. V. Reddy, M. G. Heisler, D. W. Ehrhardt, E. M. Meyerowitz, *Development* **131**, 4225 (Sep, 2004).
S6. P. B. de Reuille, I. Bohn-Courseau, C. Godin, J. Traas, *Plant J* **44**, 1045 (Dec, 2005).
S7. W. Flugge, *Stresses in shells*. (Springer-Verlag, New York ed. 2nd ed. , 1973).
S8. C. Wei, P. M. Lintilhac, J. J. Tanguay, *Plant Physiol* **126**, 1129 (Jul, 2001).

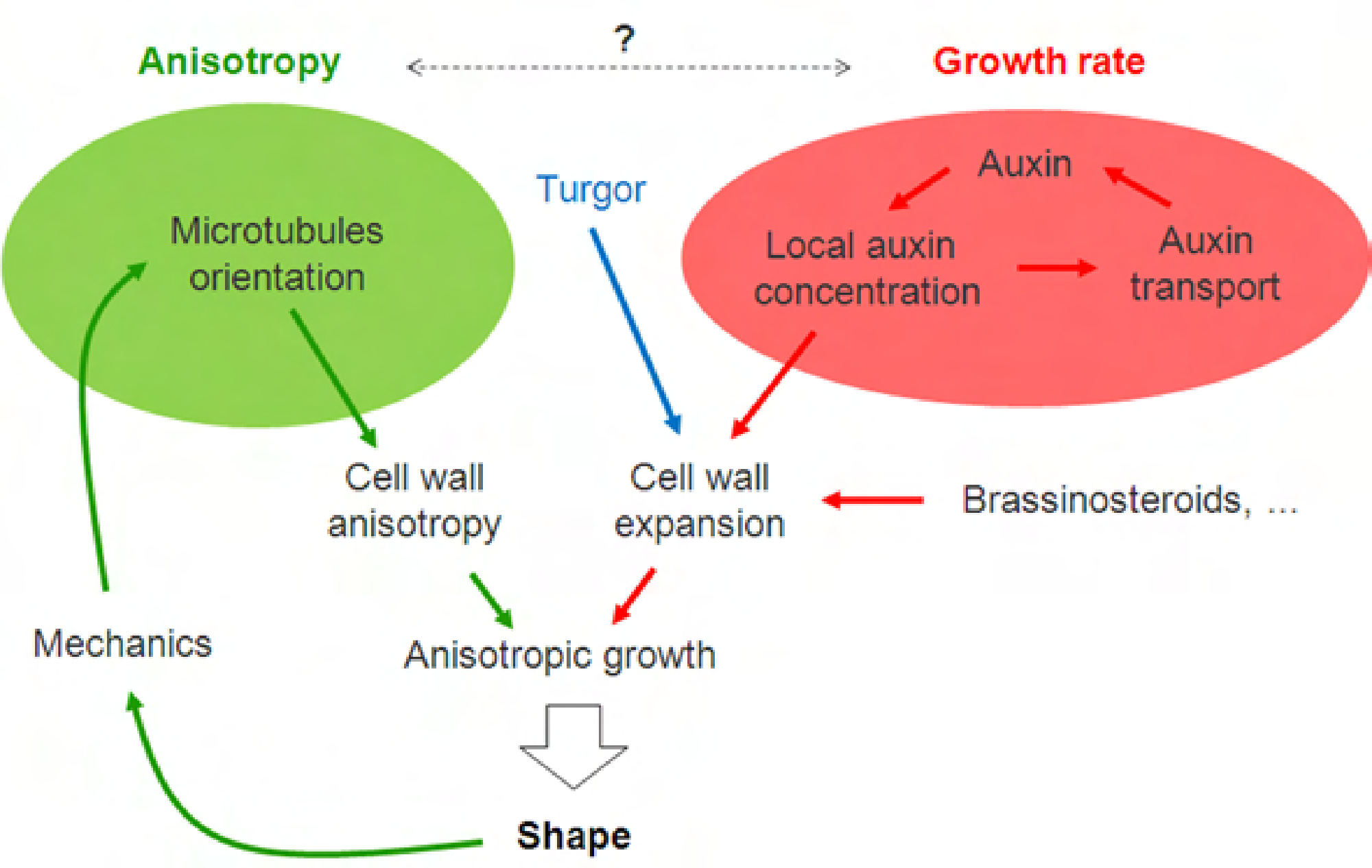
Anisotropy
?
Growth rate
Microtubules orientation
Turgor
Auxin
Local auxin concentration
Auxin transport
Cell wall anisotropy
Cell wall expansion
Brassinosteroids, …
Mechanics
Anisotropic growth
Shape

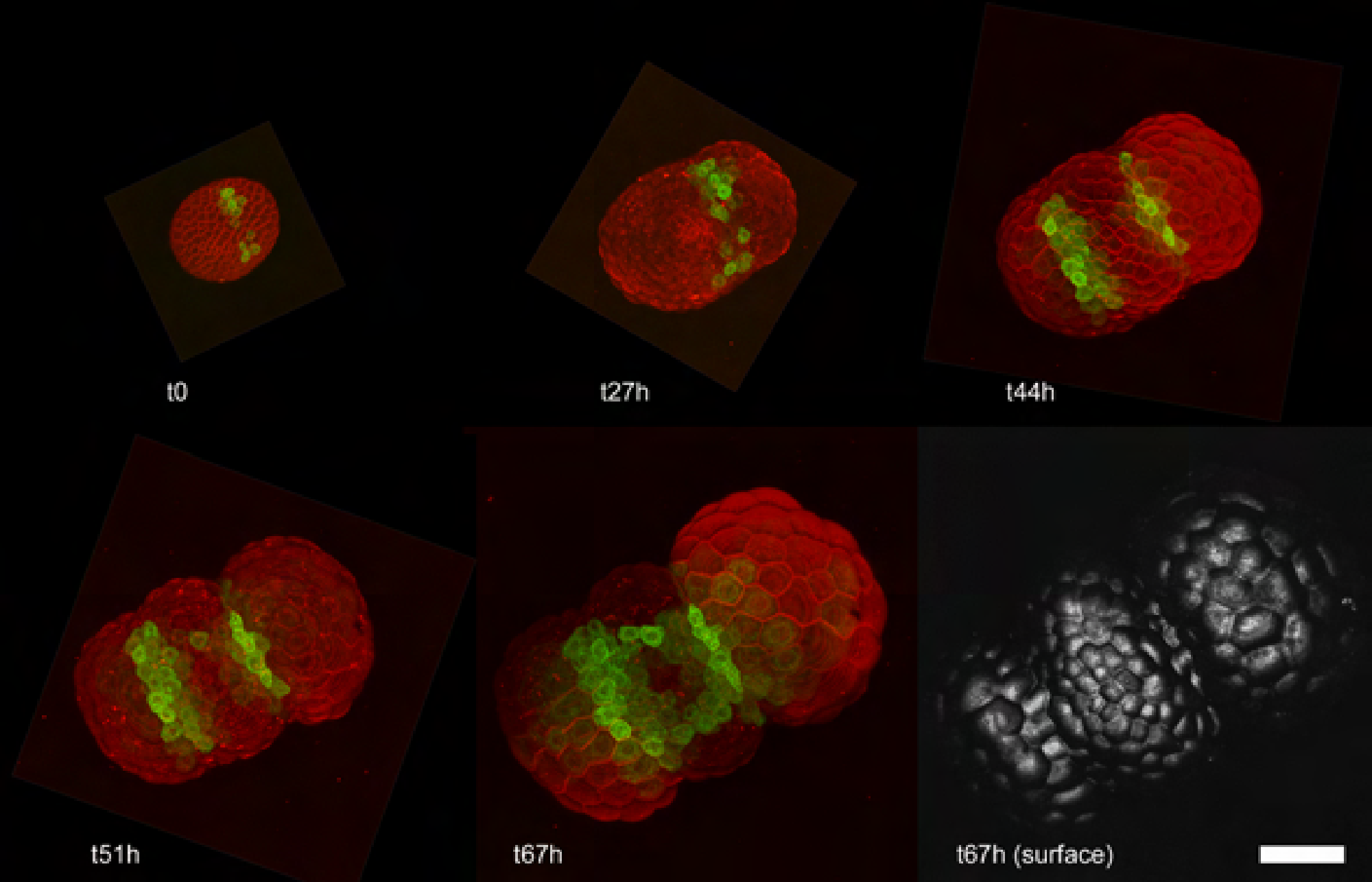
t0
t27h
t44h
t51h
t67h
t67h (surface)

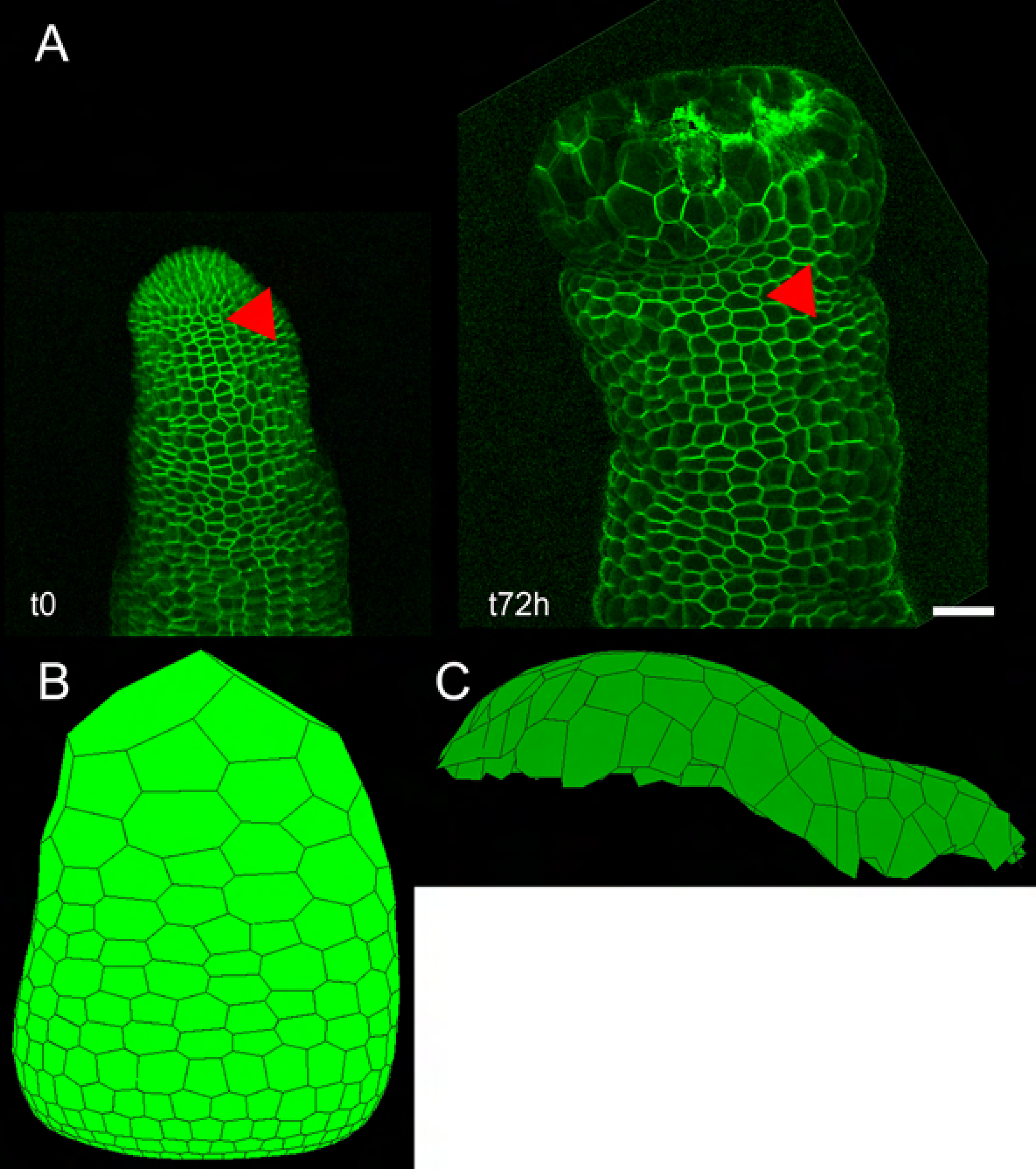
A
t0
t72h
B
C

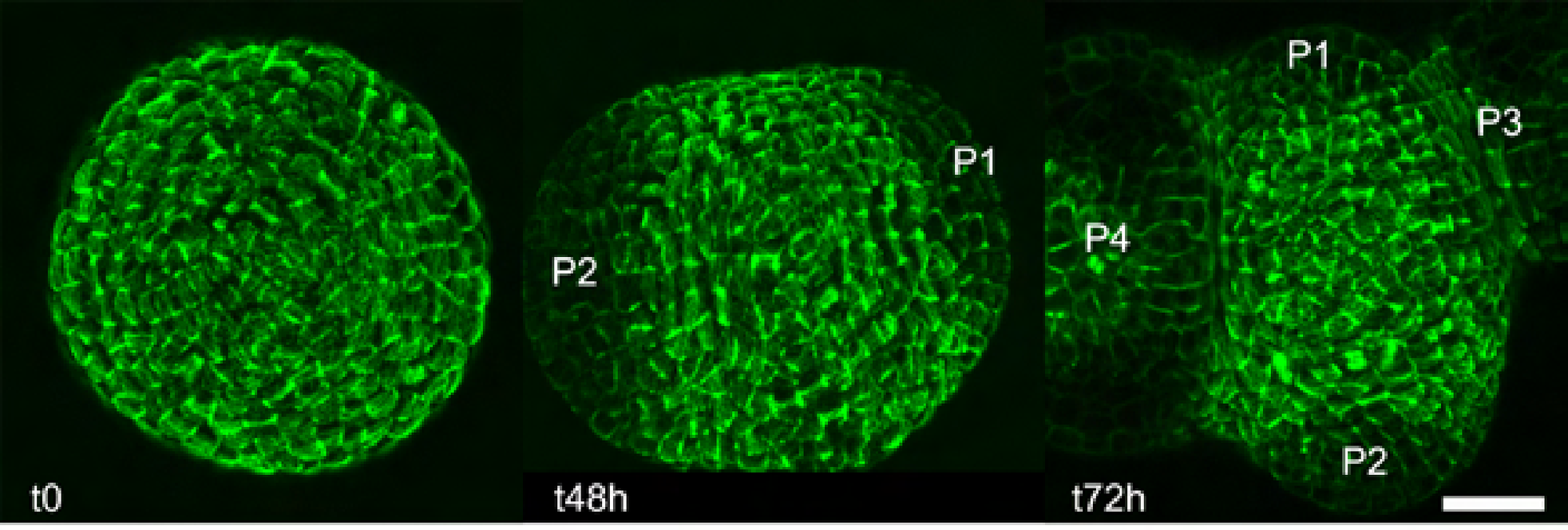

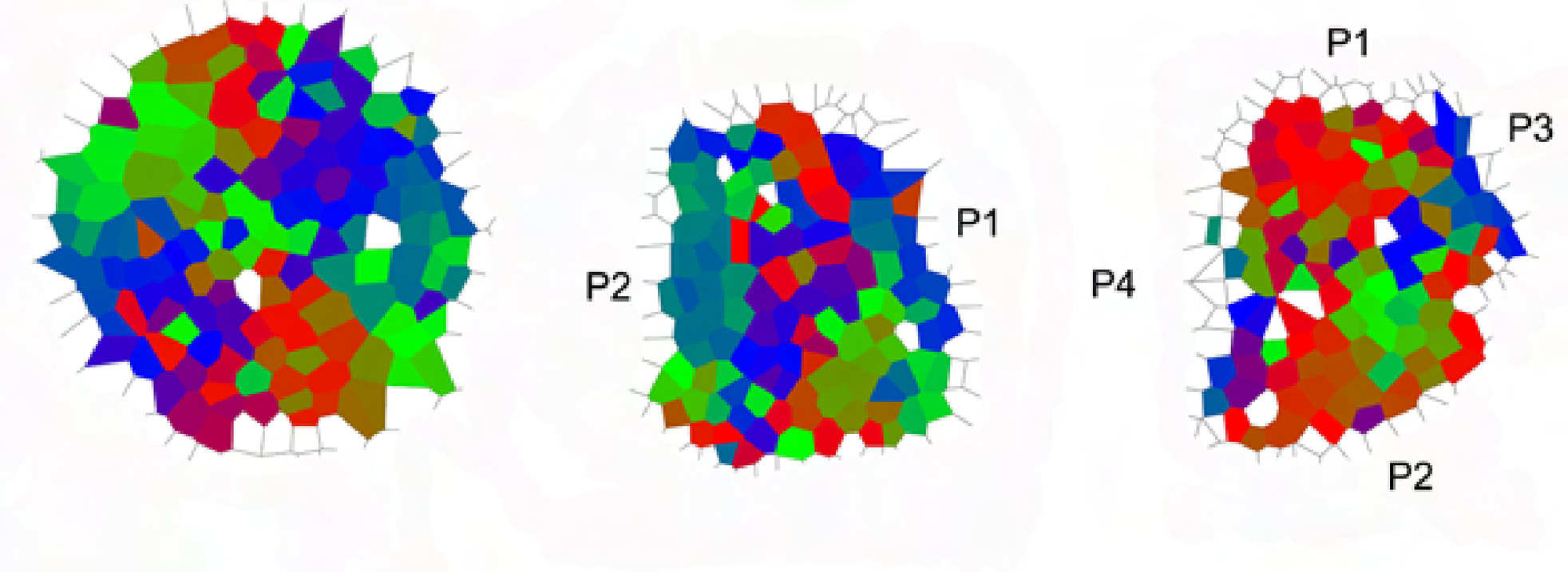

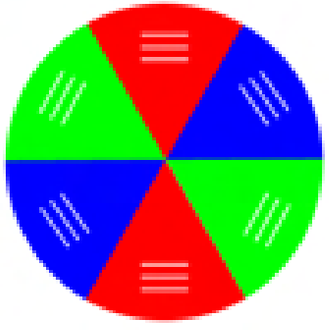

Color code
for microtubule orientations

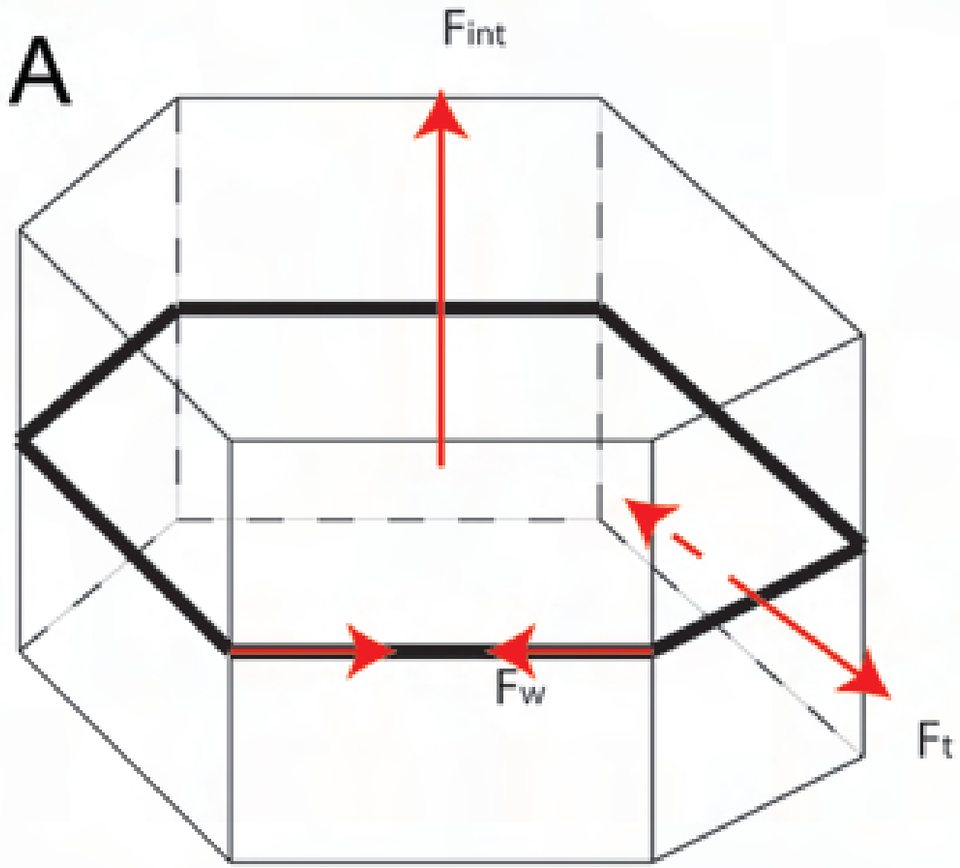
A
Fint
Fw
Ft

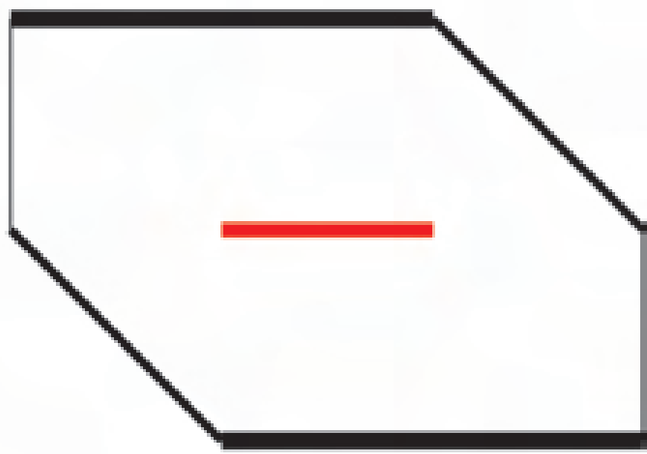
B

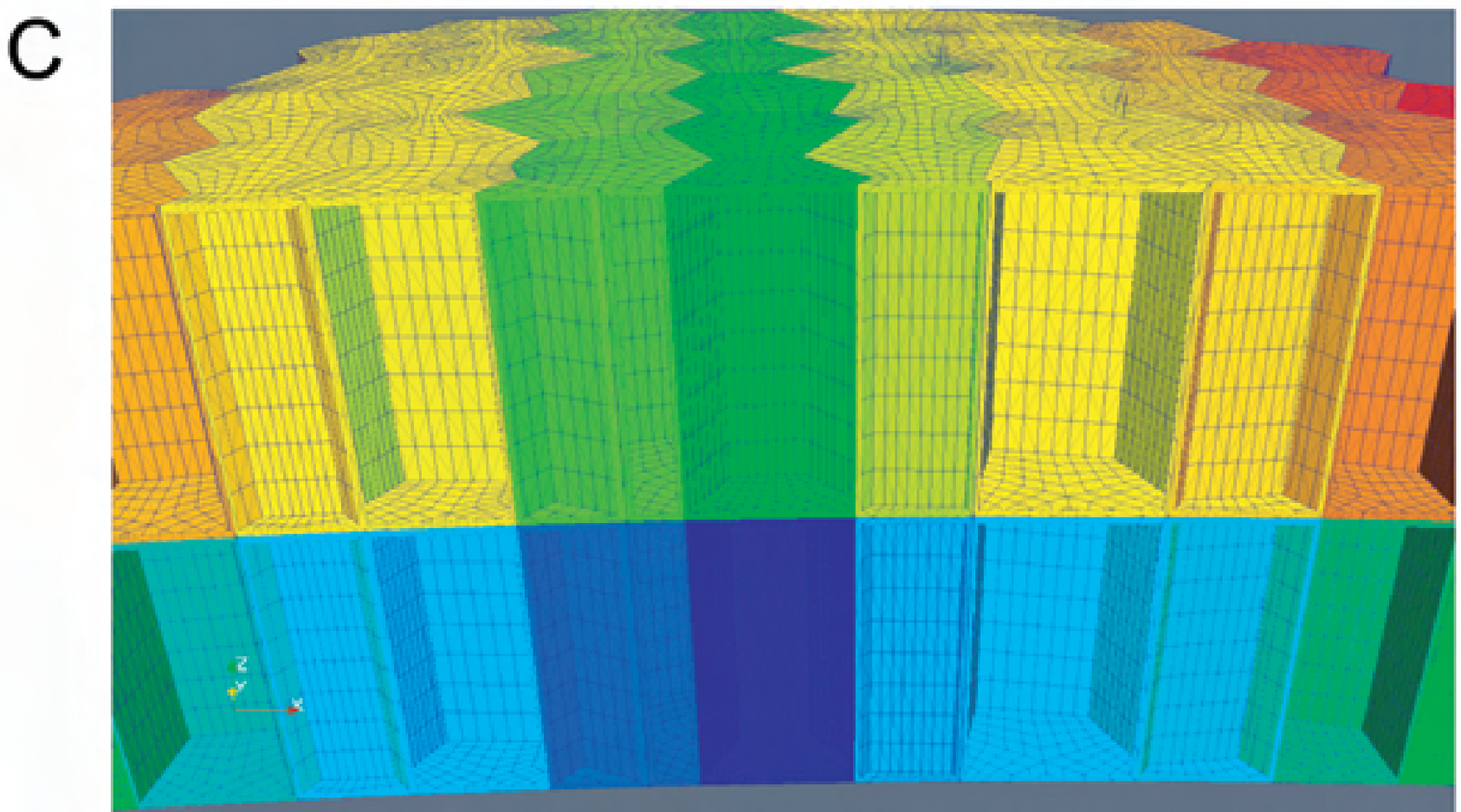
C

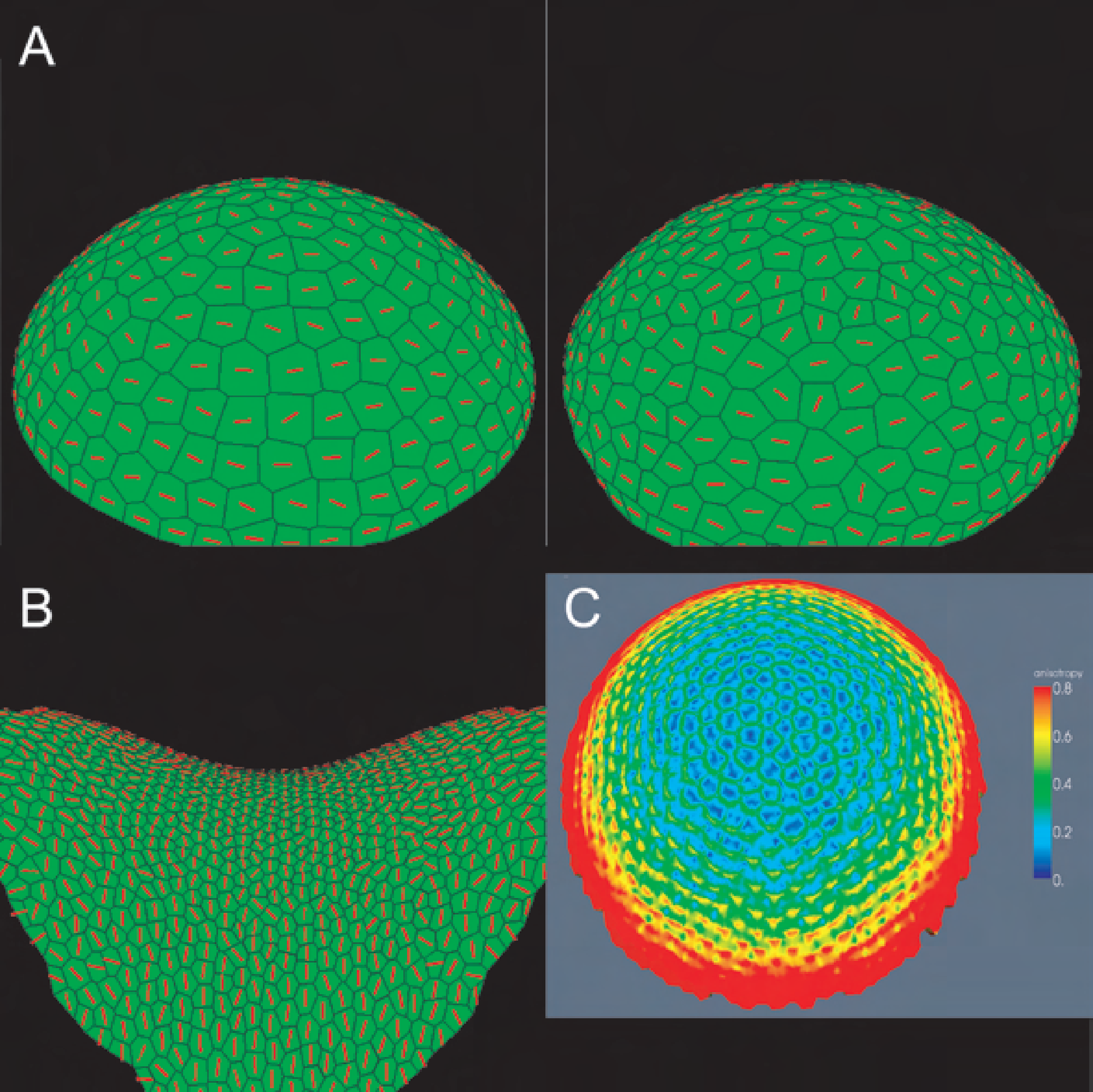
A
B
C
anisotropy
0.8
0.6
0.4
0.2
0.

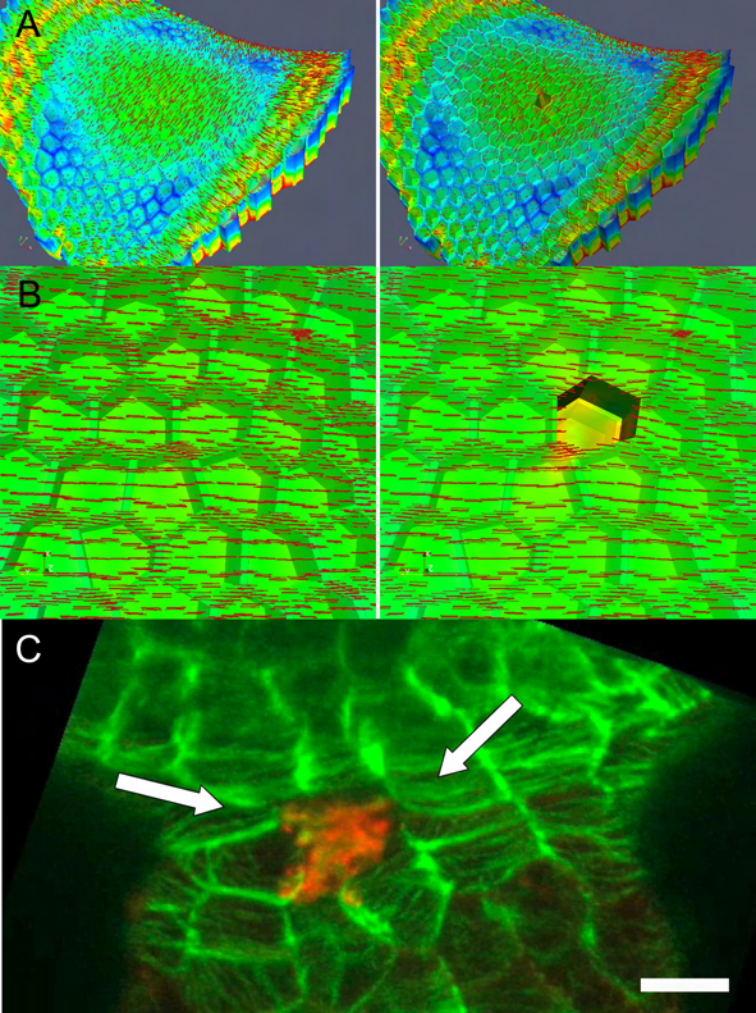
A
B
C

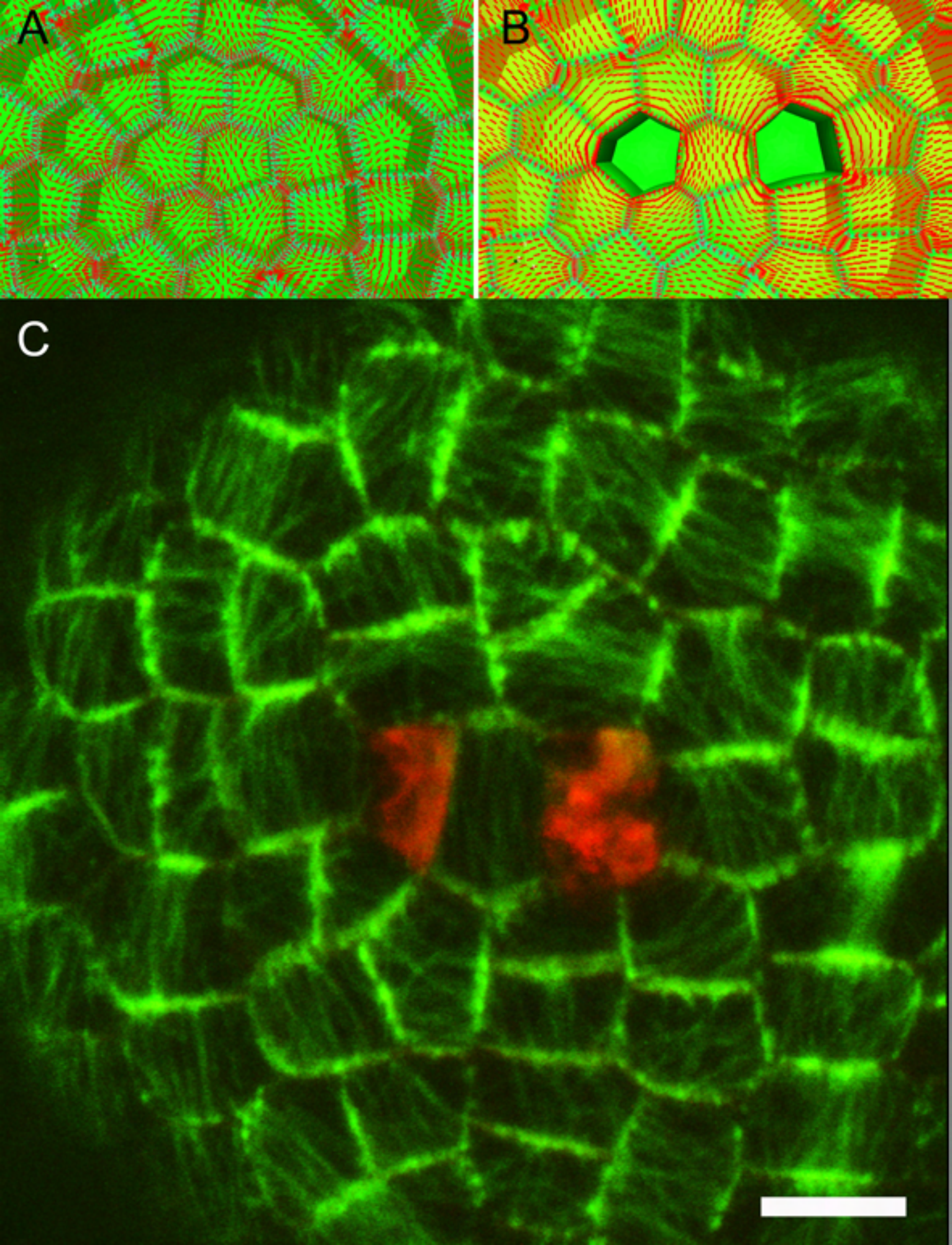
A
B
C

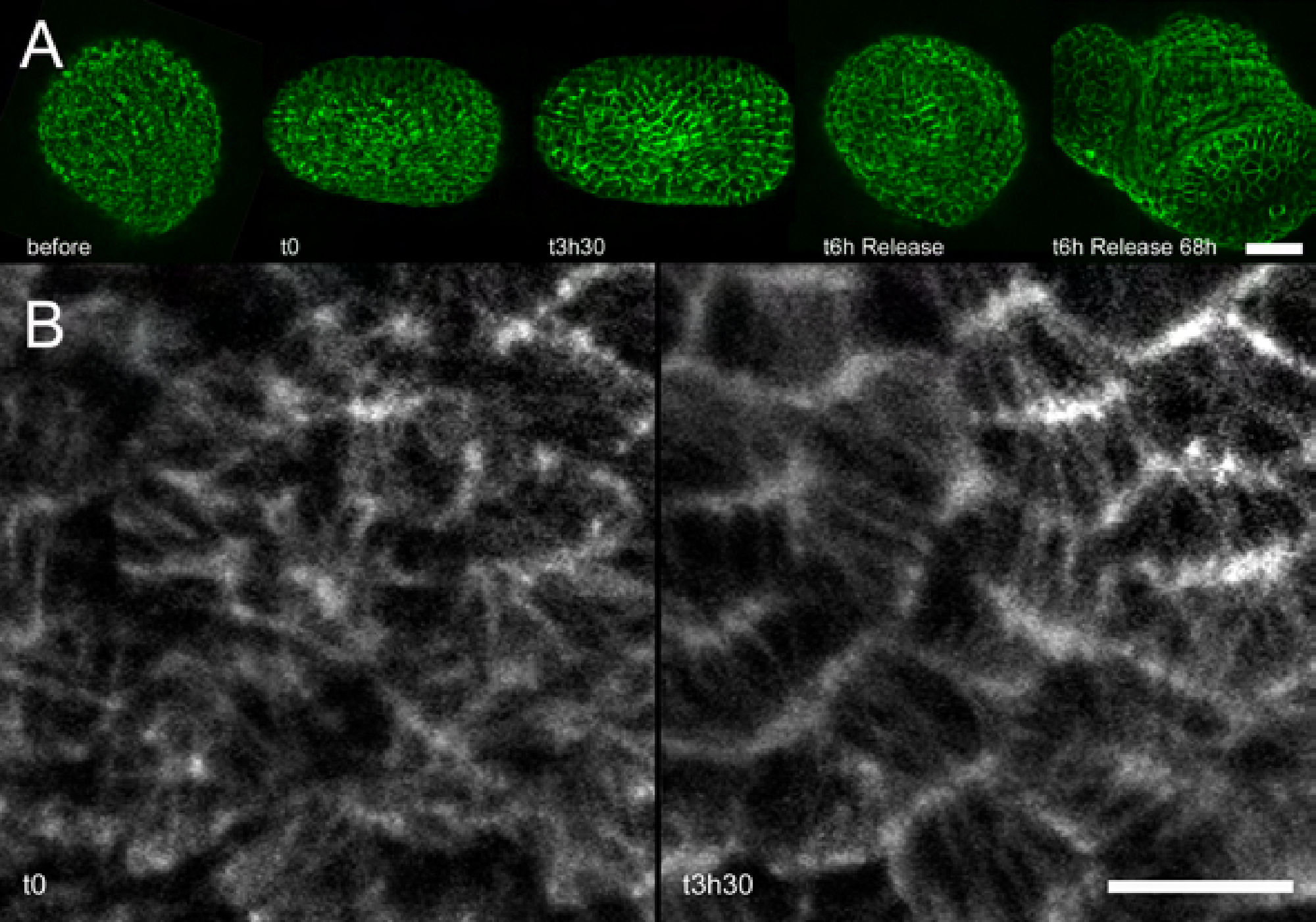
A
before
t0
t3h30
t6h Release
t6h Release 68h
B
t0
t3h30

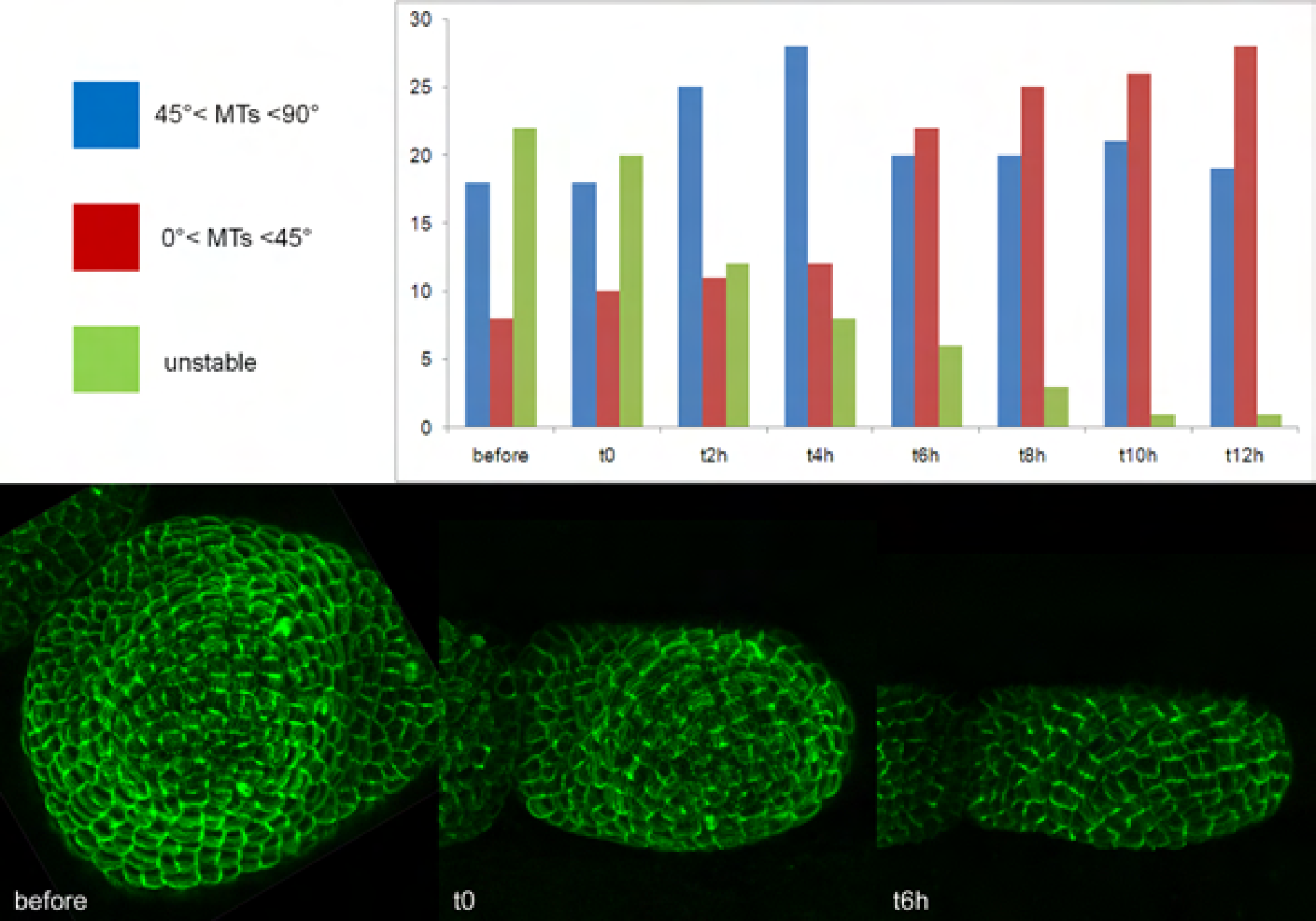
45°< MTs <90°
0°< MTs <45°
unstable
30
25
20
15
10
5
0
before
t0
t2h
t4h
t6h
t8h
t10h
t12h
before
t0
t6h

A

Microtubules reorientations after compression in cells with one main microtubule orientation at t0

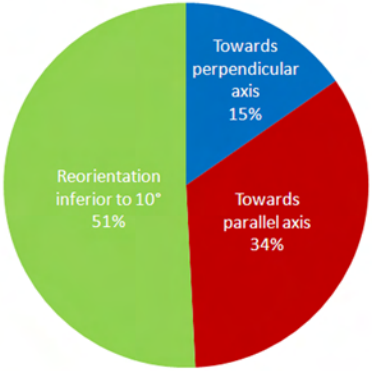

B

Microtubules orientation after compression in cells with multiple microtubule orientations at t0